ACS OMEGA

http://pubs.acs.org/journal/acsodf

Article

Simple Sonochemical Method to Optimize the Heating Efficiency of Magnetic Nanoparticles for Magnetic Fluid Hyperthermia

Jesús Antonio Fuentes-García,* Alex Carvalho Alavarse, Ana Carolina Moreno Maldonado, Alfonso Toro-Córdova, Manuel Ricardo Ibarra, and Gerardo Fabián Goya

Cite This: *ACS Omega* 2020, 5, 26357−26364

Read Online

ACCESS | Metrics & More | Article Recommendations | Supporting Information

ABSTRACT: We developed a fast, single-step sonochemical strategy for the green manufacturing of magnetite (Fe_3O_4) magnetic nanoparticles (MNPs), using iron sulfate ($FeSO_4$) as the sole source of iron and sodium hydroxide (Na(OH)) as the reducing agent in an aqueous medium. The designed methodology reduces the environmental impact of toxic chemical compounds and minimizes the infrastructure requirements and reaction times down to minutes. The Na(OH) concentration has been varied to optimize the final size and magnetic properties of the MNPs and to minimize the amount of corrosive byproducts of the reaction. The change in the starting $FeSO_4$ concentration (from 5.4 to 43.1 mM) changed the particle sizes from (20 ± 3) to (58 ± 8) nm. These magnetite MNPs are promising for biomedical applications due to their negative surface charge, good heating properties (≈324 ± 2 W/g), and low cytotoxic effects. These results indicate the potential of this controlled, easy, and rapid ultrasonic irradiation method to prepare nanomaterials with enhanced properties and good potential for use as magnetic hyperthermia agents.

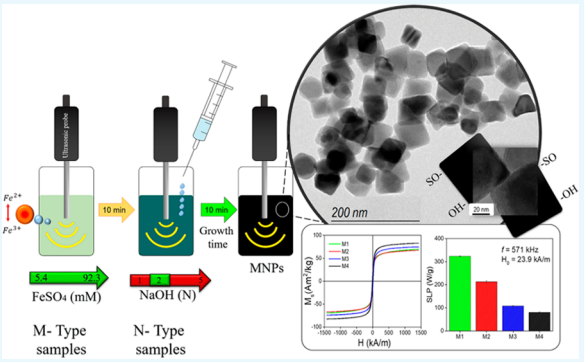

INTRODUCTION

The sonochemical route is one of the simplest methods of obtaining magnetic materials.[1,2] First reported in the 1980s for the organic synthesis of β-alkylated ketones through the Barbier reaction,[3] the application of sonochemical methods has evolved from the initial ultrasonic irradiation of aqueous binary solutions[4] into a well-established method of preparing nanostructured materials.[5] The mechanism that allows sonochemistry in a solution is acoustic cavitation, i.e., the fast growth and subsequent implosive collapse of gas bubbles within the liquid phase.[6] The collapse of bubbles can generate localized hot spots with transient temperatures up to 5000 K and cooling rates of $>10^3$ K/s.[7] This production of hot spots and cavitation (primary sonochemistry) triggers the production of oxidant radicals (secondary sonochemistry), promoting the reaction to yield the final stable phases.[8] Ultrasonic irradiation promotes improved solute diffusion; therefore, the induction time and metastable zone width are reduced, the nucleation rate is increased, and the crystallization process is enhanced.[9]

In addition, vigorous microscale mixing and turbulence helps to prevent crystal agglomeration (especially for magnetic nanoparticles) and, for those crystals with sizes smaller than the resonant size of the bubble, the shockwave generated by acoustic cavitation causes particle collisions and fragmentation.[10] However, the mechanisms of sonocrystallization and sonofragmentation are not yet completely understood.[11] The main parameters determining the final materials are the ultrasonic frequency, intensity,[12] and the influence of the solvent properties in a solution, such as the vapor pressure, viscosity, or superficial tension.[13] To reduce the consumption of chemical reagents while optimizing the properties of the magnetic nanoparticles (MNPs) for a greener processing strategy, a key step is the systematic study of the reactant's concentration. Previous reports on the sonochemical synthesis of Fe_3O_4 MNPs have been based on the use of a considerable amount of ecotoxic precursors, such as iron hydroxide ($Fe(OH)_2$),[14] iron pentacarbonyl ($Fe(CO)_5$),[15] or iron chlorides.[16] On the other hand, those few works using the much less ecotoxic iron sulfate ($FeSO_4$) as a precursor well controlled the properties of Fe_3O_4 MNPs at the expense of a high irradiation power (1500 W) and required postsynthesis thermal annealing for 1 h.[17] Sonochemical methods could represent a new option as an industrial-scale, easy, and green methodology.[18−22] Different efforts reported in the literature

Received: May 12, 2020
Accepted: September 15, 2020
Published: October 7, 2020

showed the effect of different parameters, including the solvent used for modification,[23] ultrasound frequency,[24] and composition of precursors.[25,26] However, more experimental evidence of the efficiency and systematic studies to achieve a better understanding of the phenomena are still needed.[27]

In this work, we report the results of a proposed aqueous methodology used for the green manufacturing of Fe_3O_4 MNPs with controlled sizes, well-defined shapes, and suitable magnetic properties for biomedical, drug delivery, and hyperthermia applications. The strategy of producing magnetite nanoparticles with a reduced time and optimized reagent amounts allows the minimum concentration of the reductor to be obtained for controlling the size and shape; in addition, the size of the Fe_3O_4 MNPs increases as the $FeSO_4$ concentration increases, and the MNPs retain a cube-like morphology. Enhanced magnetic properties, reduced cytotoxicity, and Néel-responsive heating properties with a good specific loss power (SLP) were obtained in gelatine (≈324 ± 2 W/g) for hyperthermia applications. By combining the ultrasonic irradiation effects and the parametric optimization of Fe_3O_4 MNP synthesis, the proposed sonochemical method can be considered an option for the rapid and easy preparation of magnetic nanomaterials. The experiments in this work were conceived to improve specific loss power (SLP) values controlling nanoparticle's size and shape. The synthesis time and SLP had been optimized to show the influence of multiparametric modification in sonochemical synthesis. Optimal time and sodium hydroxide concentration allow reducing the iron sulfate amount for improved SLP. These modifications of different parameters in the simple conditions that we proposed and their influence on SLP values in a gelatine medium and their biocompatibility in vitro have not been reported in the literature.

RESULTS AND DISCUSSION

The basic protocol used to investigate the best condition for obtaining MNPs in less time (20 min in total) consisted of systematic modification of each synthesis parameter, namely, the concentration of the Na(OH) base (N-type samples) and concentration of $FeSO_4$ (M-type samples), used as a tuning agent. The proposed optimization of the growth time selected in our protocol (10 min) minimizes sonofragmentation and promotes the proper formation of uniform MNPs.

The particles prepared with better control of the shape were obtained using a 2 N solution (Figure S1) in the N-type series. However, the used concentration of $FeSO_4$ was apparently too high and did not offer size control, and at 5 N, remarkable nail-type structures appeared. Using the 2 N Na(OH) solution as the reducing agent, a screening of the $FeSO_4$ concentration was started from 5.4 to 43.2 mM for the M-type samples. We observed a remarkable improvement in the average particle size from 20 ± 3 to 58 ± 8 nm, and the particles retained the cube-like morphology (see Figure 1).

The observed influence of the initial $FeSO_4$ concentration on the size and morphology of the resulting MNPs can be attributed to the critical Fe^{2+} and Fe^{3+} abundance during the oxidation steps. The $FeSO_4$ precursor provides the required local concentration at the cavitation spots for the growth of MNPs during the short reaction time. $FeSO_4$ continuously deprotonates, supplying Fe^{2+} and with the addition of hydroxyl ions (OH^-) from NaOH, forms iron(II) hydroxides, ($Fe(OH)_2$) forming goethite as a crystal growth template.[28] Besides, within the nanoenvironment of MNPs, the electro-

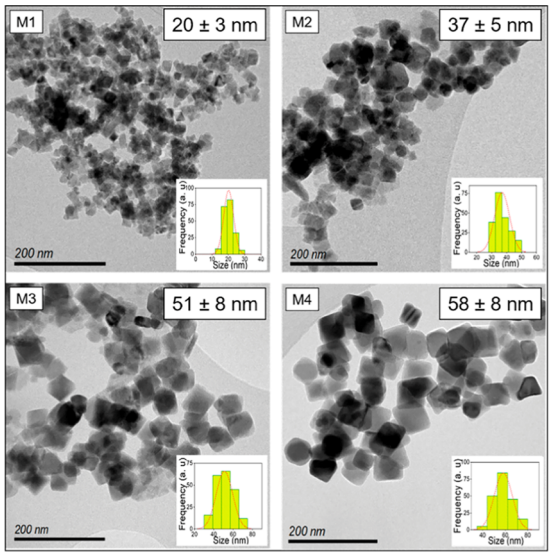

Figure 1. Transmission electron microscopy (TEM) images of the M1, M2, M3, and M4 samples, and the corresponding size distribution histograms (insets), showing the increase in the average particle sizes with increasing the initial $FeSO_4$ concentration.

chemical Stern double layer can be described as a fixed layer of surface charges and a second, external layer of counter ions. The thickness of the outer layer, and hence the local vicinity of the NPs, is highly dependent on the solution's ionic strength. This leads to a screening of surface charges accompanied by a reduction of the electrostatic stability and induces MNP agglomeration owing to dominant van der Waal's attraction. Changes in the ion concentration in the solution can influence the shape, growth, and the final size of the MNPs.[29] The ionic strength defined as $I = \frac{1}{2}\sum_i c_i z_i^2$ (where z_i represents the valence of ions of ith species and c_i $[M]$ its concentration) increases with either larger concentration or valence of counter ions. Therefore, the larger ionic strengths in more concentrated starting solutions are likely to produce thinner double layer around MNP's seeds and thus increase potential gradient. It is important to highlight that increasing the initial concentrations of $FeSO_4$ over 43.2 mM did not improve the morphology nor the size distribution of the resulting particles, suggesting a saturation effect, reducing ion's mobility, and reactivity in the solution.

The composition of the M-type samples was evaluated using Fourier-transform infrared spectroscopy (FTIR) and X-ray photoelectron spectroscopy (XPS) techniques. First, the FTIR spectra of all of the samples, M1−M4 (Figure 2a), show a broad band centered at 3420 cm^{-1}, which is due to the coordinated O−H groups in the stretching mode, and the localized peak at 1630 cm^{-1} corresponds to free surface OH− groups, as expected in synthesis routes that use Na(OH) as the reducing agent in aqueous media.[30] The peaks attributed to the S═O stretching modes of sulfate and sulfoxide groups can be observed at 1350 and 1030 cm^{-1}, respectively.[31,32] The presence of these bands suggests the presence of residual sulfate ions that were not removed in the washing process. We observed that a pH of 7 was not enough to eliminate the residual sulfate reagents in the aqueous medium; nevertheless, residual sodium from the NaOH reducing agent was not detected. The iron oxide peaks at 572 cm^{-1} in the spectra of the M2, M3, and M4 samples are associated with the magnetite

https://dx.doi.org/10.1021/acsomega.0c02212
ACS Omega 2020, 5, 26357−26364

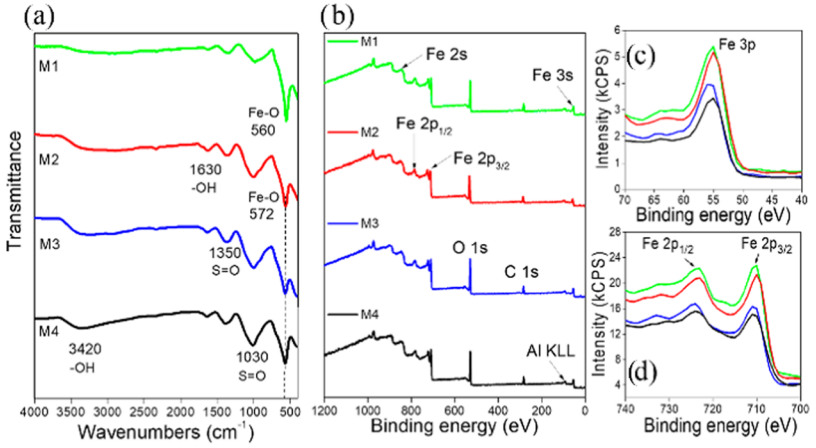

Figure 2. (a) FTIR spectra of the M1−M4 samples. The M1 spectrum is slightly shifted with respect to the spectra of the M2−M4 samples, which suggests changes in the oxidation state of iron. (b) XPS spectra of the M1−M4 samples. We can observe the presence of iron oxide, adventitious carbon, and aluminum in the sample. The close-up in (c) shows the iron oxidation states as Fe 3p due to the peak at 55 eV and (d) Fe $2p_{1/2}$ due to the peak at 723 eV and Fe $2p_{3/2}$ due to the peak at 710 eV.

phase, and the peak at 560 cm^{-1} in the spectrum of the M1 sample is attributed to the hematite phase.[33] This shift may be due to increased oxidation in the M1 sample, as the aqueous media and the presence of oxygen during synthesis can contribute to surface oxidation. This result agrees with the magnetic properties and SLP values obtained.

The XPS spectra of samples M1−M4 are shown in Figure 2b. The determination was performed using the method reported by Yamashita and Hayes.[34] As a general trend, the peak characteristics of the Fe_3O_4 phase, namely, the peaks at 846 eV (Fe 2s), 723 eV (Fe $2p_{1/2}$), 710 eV (Fe $2p_{3/2}$), and 55 eV (Fe 3s), are observed.[35,36] The typical O 1s binding energy was observed at 532 eV, while the presence of adventitious carbon was inferred from the peak detected at 284 eV. The small peak at 97 eV is associated with aluminum (Al KLL). We hypothesize that the presence of aluminum in the resulting particles may be due to slight Al-doping due to the dissolution of some metallic ions from the Ti−6Al−4V alloy ultrasonic irradiation tip used in the synthesis. Figure 2c shows the peak at 55 eV, which corresponds to the Fe 3p interaction, showing slight changes in the binding energy, implying negligible oxidation changes. Figure 2d shows that the M1 sample undergoes some changes in Fe $2p_{1/2}$ and Fe $2p_{3/2}$ and shows the presence of satellite peaks at 718 eV, and the atomic Fe^{2+}/Fe^{3+} ratios can be observed in Table S3. These changes are associated with the Fe_2O_3 phase and match the FTIR characterization results. The increase in Fe^{3+} in the M2−M4 samples corresponds to better crystallization in the Fe_3O_4 phase. The localized Fe 3p peak at 55 eV for the M4 sample and the absence of the satellite peak support this.

The magnetic data of the M1−M4 samples (Figure 3a and Table 1) showed that the values of M_S and H_C were consistent with the Fe_3O_4 nanostructured phase. The H_C value of the M1 sample (5.33 kA/m or 67.0 Oe) was less than that of multidomain Fe_3O_4 ($H_C \approx 11.93$ kA/m or 150 Oe)[37] at room temperature, suggesting that at least a fraction of the smallest MNPs exhibit a superparamagnetic behavior, while the M2−M4 samples have larger H_C values than M1, indicating that samples M2, M3, and M4 are closer to being multidomain due to their increasing sizes. The magnetic properties of the M-type samples suggest the strong influence of $FeSO_4$ modification on the formation of well-defined, crystalline MNPs using the

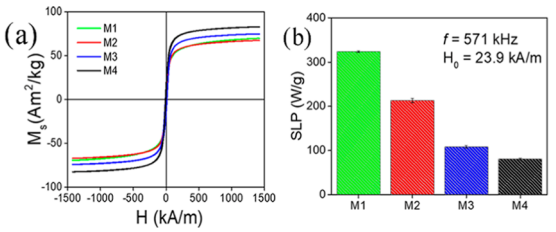

Figure 3. (a) Magnetization curves obtained for samples M1−M4, and (b) measured SLP values (H_0 = 23.9 kA/m, f = 571 kHz) obtained in a gelatine matrix, in which Brownian relaxation is blocked.

proposed sonochemical synthesis method. The amount of the precursor in the aqueous solution can modify M_S and H_C and make it possible to obtain superparamagnetic properties at low $FeSO_4$ concentrations.

Table 1 shows the effective magnetic anisotropy (K_{eff}) of each sample, as obtained from ferromagnetic resonance spectroscopy (FMR). The effective magnetic anisotropy determines the magnetic relaxation mechanism of the MNPs and is the key parameter when the physical rotation of the particles is blocked, as is the situation for in vitro and in vivo magnetic fluid hyperthermia applications. The heating efficiency is measured through the specific loss power (SLP), which is the power absorbed per gram of material under radiofrequency irradiation. The values of K_{eff} obtained from the FMR measurements of the oriented samples also reflect the evolution of the series of samples from poorly crystallized to well-crystallized magnetic cores, since the K_{eff} values increase by a factor of 5 from the M1 sample to the M4 sample. Indeed, the K_{eff} value of the M1 sample (2.4 kJ/m^3) is significantly lower than the magnetocrystalline anisotropy of bulk magnetite ($K_1 = -11.1$ kJ/m^3), which is consistent with the presence of partially formed Fe_3O_4 and/or the presence of intermediate oxyhydroxide phases of iron, which has a much lower magnetic anisotropy than bulk magnetite. As the formation of crystalline magnetite occurs from M1 to M4, the magnetic anisotropy of the nanoparticles reaches a K_{eff} value = 10.5 kJ/m^3, which is expected for bulk Fe_3O_4.

For hyperthermia applications, the heating power of MNPs depends critically on the average particle size, but other factors such as the particle shape and magnetic anisotropy also

https://dx.doi.org/10.1021/acsomega.0c02212
ACS Omega 2020, 5, 26357−26364

Table 1. Main Physical Parameters of the Nanoparticles Obtained[a]

sample	$\langle d \rangle$ (nm)	σ (nm)	ξ (mV)	M_S (A·m^2/kg)	H_C (kA/m)	K_{eff} (kJ/m^3)	SLP (W/g)
M1	20	3	−2.1	70	5.33	2.4	324 ± 2
M2	37	5	−13.2	67	10.34	5.4	213 ± 5
M3	51	8	−16.1	75	11.69	5.8	108 ± 3
M4	58	8	−33	85	11.22	10.5	81 ± 2

[a]Average particle size ($\langle d \rangle$), distribution of the standard deviation (σ), ζ-potential (ξ), saturation magnetization (M_S), coercive field (H_C), anisotropy constant (K), and specific loss power (SLP).

determine the sizes that maximize the SLP. Specifically, for the Fe_3O_4parameters, it is expected that the optimum sizes for heating should be approximately 25−30 nm, depending on the K_{eff} and shape properties of a specific sample. Consistently, the SLP values of the M1−M4 series of samples (Figure 3b) showed a maximum SLP = 340 W/g for the M1 sample, and the SLP decreased in the order of M1 > M2 > M3 > M4, as the average particle size increases from M1 to M4 (20−58 nm). We note that all power absorption measurements were performed in samples with nanoparticles embedded in a gelatine matrix to avoid the physical rotation of the MNPs (i.e., to avoid Brownian relaxation and measure only Néelian magnetic relaxation). The purpose of measuring only Néel relaxation is to mimic the actual in vitro or in vivo environmental conditions, so the MNPs are unable to rotate (see the Characterization Section of the Supporting Information for details of sample preparation). The evolution of the SLP from the M1 to M4 samples is shown in Figure 3. The observed SLP decrease is consistent with the simultaneous increase in the average size of the MNPs and their effective anisotropy K_{eff}, as the (anisotropy) energy barrier for magnetic relaxation $E_a = K_{eff}V$ results in extremely large values of the magnetic relaxation time.

The SLP value of 60 W/g of the sonochemically synthesized MNPs recently published in the literature[38] was evaluated in aqueous media that included Brownian contributions. Recent advances in the experimental observation of the Néel relaxation contribution in Fe_3O_4 MNPs obtained by thermal decomposition (<20 nm) in a clinical setting (H = 16.2 kA/m; f = 110 kHz) show decreasing SLP values from 67 W/g in a solution to 25 W/g in a gel medium.[39] On the other hand, spherical Fe_3O_4 (<14 nm) obtained by a chemical route shows a decreasing dependence on heat dissipation in agar media. The SLP values decreased from 200 to 140 W/g as the agar concentration increased (<7%).[40] We can observe that the SLP values in this work are higher than those recently reported, even when the MNP concentration in gelatine is 10 w/v, which suggests a higher viscosity. This can be associated with the larger field strength used in this study; however, the SLP obtained in this study is comparable to the literature value of 279 W/g of polyacrylic acid-coated MNPs in a cell culture at the same field conditions.[41]

Iron oxide magnetic nanoparticles, especially magnetite (Fe_3O_4) and maghemite (γ-Fe_2O_3), are usually reported as being "nontoxic" and biocompatible. The cytotoxicity and biocompatibility of MNPs are intrinsically related to MNP physicochemical characteristics, including the chemical composition, size, shape, charge, superficial area, aggregation, and functionalization.[42] Therefore, it is necessary to determine the toxicity both in vitro and in vivo for each nanoparticle formulation if biomedical applications are pursued. As shown in Figure 4, no significant cytotoxicity was observed after a 2 h exposure to MNPs with concentrations up to 200 μM, which shows the remarkable biocompatibility of samples M1−M4 in this particular cell line.

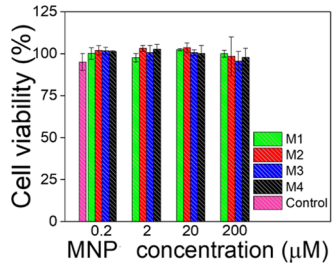

Figure 4. Viability of mouse microglia cell line (C57BL/6) in the presence of different concentrations of Fe_3O_4 MNPs synthesized by the ultrasonic process. The synthesized MNPs show a remarkable biocompatibility until a 200 μM concentration.

The increase in particle size from 20 to 58 nm through samples M1−M4 does not seem to play a key role in their toxicity, which is consistent with other reports in the literature, where no relationship has been found between cytotoxicity and particle size differences from nanometers to micrometers.[43] Depending on the nature of the synthesized particles, other parameters like shape, surface chemistry, oxidation status, or agglomeration rather than particle size could have a greater impact on their cytotoxic profile.[42] For example, positively charged particles are generally more cytotoxic than neutral or negatively charged particles since they can penetrate deeper into cell membranes. Also, rod-like-shaped particles present more toxicity than cubic and spherical particles. In our case, all samples present a good control over a cube-like shape and negative values of ζ-potential. Furthermore, the presence of OH^- and SO_4^- ions on the surface could probably reduce the reactivity of surface iron ions, generating less ROS and oxidative stress, which is the main mechanism of SPION cytotoxicity.[44,45] Together, these parameters could explain the absence of toxicity observed for all of the four samples.

CONCLUSIONS

The possibility of producing MNPs with controlled properties through all-in-one methods is appealing. The optimization of the sonochemical synthesis reported here provides such a method, combining cheapness, easiness, high throughput, biocompatibility, and environmental friendliness. Moreover, the method allows control of the uniformity of the size and shape of the produced MNPs within the ≈20−60 nm range. As expected in this size range, the best SLP values (Néel contribution only) were displayed for poorly crystallized nanoparticles, which provides an additional route for maximizing the heating capacity of the produced nanoparticles. Under the conditions tested here, a maximum SLP value of 324 ± 81 W/g was found. The "in vitro" study probes the good toxicity levels. The abovementioned properties situate this

https://dx.doi.org/10.1021/acsomega.0c02212
ACS Omega 2020, 5, 26357−26364

synthesis route among the most promising alternatives for future commercial-scale biomedical applications.

EXPERIMENTAL SECTION

Materials. The chemical reagents used in the synthesis were iron (II) sulfate heptahydrate ($FeSO_4{\cdot}7H_2O$ ≥99%), sodium hydroxide (Na(OH) ≥97%), ammonium thiocyanate (NH_4SCN, ACS reagent, ≥97.5%), hydrochloric acid (HCl, ACS reagent, 37%) and nitric acid (HNO_3, ACS reagent, 70%) purchased from Sigma-Aldrich and used as received. Deionized water (Millipore 18.2 MΩ·cm) was used in all experiments. Continuous ultrasonic irradiation at 3.6 W/cm^2 was generated using an Ultrasonic Vibra-cell VCX 130 processor with Ti−6Al−4V (6 mm) tip. We used a laboratory borosilicate glass bottle (ϕ = 56, h = 100 mm) with a capacity of 100 mL as a reactor. For in vitro studies, Dulbecco's modified Eagle's medium (DMEM), fetal bovine serum (FBS), antibiotic−antimycotic (100×), DNase/RNase-free water, Dulbecco's phosphate-buffered saline (DPBS), trypsin solution (0.25%), and trypan blue solution (0.4%) were all purchased from Thermo Fischer Scientific (Waltham, MA).

Protocol for the Synthesis of Nanoparticles. The sonochemical route used in this work is based on the method reported by Abbas et al.[17] in 2012, and modified as described below. This method profits from the oxidizing species produced by secondary sonochemistry as follows

$$H_2O \rightarrow H^+ + OH^- \quad (1)$$

$$H^+ + H^+ \rightarrow H_2 \quad (2)$$

$$OH^- + OH^- \rightarrow H_2O_2 \quad (3)$$

And subsequent partial oxidation of the Fe^{2+} ions from the $FeSO_4$ by H_2O_2

$$Fe^{2+} + H_2O_2 \rightarrow Fe^{3+} + 2OH^- \quad (4)$$

This mechanism provides both Fe^{2+} and Fe^{3+} ions required for magnetite from a single iron source, i.e., the starting $FeSO_4$. As expected, the pH of the solution is critical to control the partial oxidation yielding to the correct Fe(II)/Fe(III) required for the formation of magnetite. Different bases such as sodium hydroxide (Na(OH)) are commonly used to saturate anions OH^- and promote the formation of Fe_3O_4 as the following reaction

$$Fe^{2+} + 2Fe^{3+} + 8OH^- \rightarrow Fe_3O_4 + 4H_2O \quad (5)$$

The effects of the initial concentrations of the reducing agent (Na(OH)) and the reactant ($FeSO_4$) were systematically screened. First, the precursor concentration was fixed and different Na(OH) concentrations (N-type samples) were added, and second time different precursor concentrations were used at a fixed Na(OH) concentration (M-type samples). Figure 5 shows an outline of the proposed experiment, and Table 2summarizes the reaction parameters like concentration of $FeSO_4$ and Na(OH), and pH after Na(OH) addition (growth pH).

In the case of N-type samples, the same $FeSO_4$ solution 92.3 mM was employed. Ultrasound irradiation for 10 min at 130 W was applied to the solutions to increase the temperature of the solution (volume 90 mL) to 50−52 °C at which the ionic exchange takes place, as shown in (4). Then, different Na(OH) concentrations (0.8, 1.2, 1.6, 2, and 2.4 g) dissolved in 10 mL of H_2O were added into the flask and irradiated for additional 10 min, obtaining the samples labeled as 1N, 2N, 3N, 4N, and 5N, respectively. To assess the influence of precursor concentration, the same 90 mL volume aliquots were prepared with increasing $FeSO_4$ concentrations of 5.4, 10.8, 21.7, and 43.1 mM, with a constant amount of oxidant (10 mL of 2 N Na(OH) solution). These samples were identified as M1, M2, M3, and M4, respectively. In all cases, the obtained MNPs were cooled with 100 mL of deionized water, precipitated using a NdSmFe magnet, and washed five times using Milli-Q water to reach neutral pH.

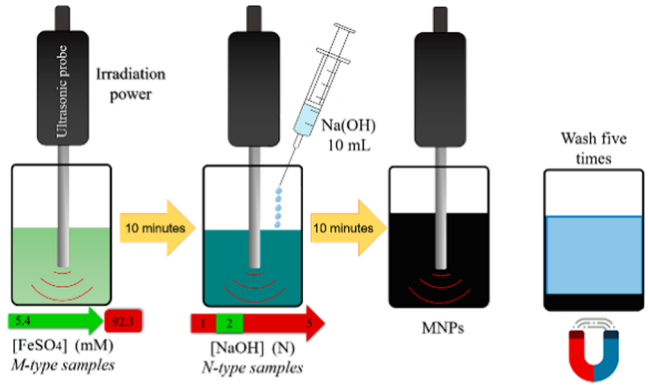

Figure 5. Schematic description of the synthesis steps for producing magnetic nanoparticles studied in this work.

Table 2. Reaction Parameters Used for Each Sample: Concentration of Reactants and Growth pH

sample	[Fe(SO_4)] (mM)	[Na(OH)] (N)	pH
1N	92.3	1	9
2N	92.3	2	13
3N	92.3	3	14
4N	92.3	4	14
5N	92.3	5	14
M1	5.4	2	13
M2	10.8	2	13
M3	21.7	2	13
M4	43.1	2	13

Characterization. *TEM.* Transmission electron microscopy (TEM) images taken using a Tecnai F30 analytical microscope (300 kV) in a bright field mode. All samples were deposited in TEM grids (Holey Carbon films on Copper) by dropping diluted aqueous dispersions of as obtained MNPs.

XPS. The XPS spectra of MNP powder obtained in the AXIS Supra (XPS) surface analysis instrument from Kratos Analytical were analyzed according to Yamashita and Hayes.[34]

FTIR. FTIR spectra were obtained in a Spectrum Two FT-IR spectrometer from Perkin Elmer at 4000 to 400 cm^{-1} interval with a resolution of 4 cm^{-1} and ATR correction. The samples were deposited directly on the glass and dried with N_2 to reduce water presence.

VSM. Magnetization hysteresis loops were measured for all samples using a vibrating sample magnetometer (VSM, Lake Shore 7400 Series) at room temperature in −1432.39 kA/m ≤ H ≤ + 1432.39 kA/m interval after drying the samples in vacuum over 24 h.

Z-Potential. For Z-potential determination of samples dispersed in Milli-Q water, a Zetasizer Nanoseries Nano-ZS90 of Malvern Panalytical was employed.

Anisotropy Determination. The effective magnetic anisotropy constant K_{eff} was measured by analyzing the angular

https://dx.doi.org/10.1021/acsomega.0c02212
ACS Omega 2020, 5, 26357−26364

dependence of the resonance field H_R in ferromagnetic resonance spectroscopy (FMR) experiments at room temperature. The FMR spectra were taken using a Bruker ELEXSYS II-E500 X-band model spectrometer at 9.4 GHz (X-band). Attenuation was set to 10 dB (20 mW microwave power) and field modulation amplitude at 0.08 kA/m. Prior to measurements, samples were aligned by dispersing the MNPs in a cyanoacrylate resin and drying the samples until complete solidification was achieved under a constant external magnetic field $H_{ext} \approx 50$ kA/m for 24 h. The acquisition of EPR spectra was performed in rotation steps of 10° covering a complete 360° turn.

Specific Loss Power (SLP). The values of MNPs heat produced were measured by triplicate using a commercial magnetic field applicator DM100 (nB nanoscale Biomagnetics, Spain) at H_0 = 23.9 kA/m, f = 571 kHz. The samples were measured after jellification in a gelatine medium at 0.1 mg/mL concentration, mixing deionized water and commercial gelatine at 60 °C. The temperature vs time curves were recorded for 2−10 min, and the SLP values were calculated using the equation[46]

$$\mathrm{SL\ P_{MNPs}} = \frac{\rho_m C_m}{\phi}\left(\frac{\Delta T}{\Delta t}\right)_{max} \quad (6)$$

where ρ_m = 1350 kg/m^3 and C_m = 4.1 kJ/kg.K are the density and specific heat of the medium (gelatine), respectively, ΔT is the temperature increment during the measuring time Δt (i.e., the slope from T vs time curve), and ϕ is the concentration of NPs in (kg of Fe_3O_4)/m^3. The experimental specific heat value was determined using a sample of the as-prepared gelatine and differential scanning calorimetry analysis was performed. The specific heat was determined using DSC Q20 (TA Instruments) and DSC Q2000 (TA Instruments) equipment. The gelatine revealed thermal stability reflected in the constant heat flow at 10−100 °C interval (Figure S1). At the same temperature interval, the specific heat measured using DSC Q2000 was found to be essentially constant within the experimental temperature range measured.

We determined iron concentration in samples by UV−Vis spectrophotometry through the thiocyanate complexation reaction, monitoring a maximum in the absorbance band centered at 478 nm wavelength using a Shimadzu UV Mini 1240 UV−Vis spectrophotometer, as reported in the literature.[47] Ammonium thiocyanate (1.5 M) was added to different samples dissolved in HCl 6M-HNO_3 (65%) at 50 °C for 2 h until the complete oxidation to Fe^{3+} ions and formation of an iron-thiocyanate complex. The absorbance of each sample compared to the calibration curve reveals their Fe content. Assuming that the obtained value of concentration corresponds to the Fe_3O_4 phase, the concentration of MNPs using the expression was calculated using the following expression

$$[\mathrm{MNPs}] = \frac{(M_{wFe_3O_4})([\mathrm{Fe}])}{3M_{wFe}} \quad (7)$$

where M_w are the molecular weights of Fe_3O_4 (231.53 g/mol) and Fe (55.84 g/mol), respectively.

Cell Viability Assay. For in vitro studies, mouse (C57BL/6) microglia cell line BV2 from ATCC (Manassas, VA) was routinely cultured into 25 cm^2 flasks in Dulbecco's modified Eagle's medium (DMEM) supplemented with 10% fetal bovine serum (FBS) and 1% antibiotic−antimycotic solution at 37 °C in a 5% CO_2 atmosphere. Prior to the experiments, as-synthesized MNPs were precipitated using a permanent magnet and resuspended in DNase/RNase-free distilled water. Cells were seeded in 12-well plates at a density of 2 × 10^4 cell/well and grown to approximately 70% of confluence. On the day of the assay, the cultured medium was replaced with a fresh medium containing different amounts of nanoparticles (0−200 μM) and further incubated for 2 h at 37 °C. After this time, cells were trypsinized, resuspended in fresh media, and diluted to 1:1 with sterile a 4% trypan blue dye solution. The hemocytometer chamber was carefully and continuously filled with this suspension and immediately counted under the microscope. Unstained (viable) and stained (nonviable) cells were counted separately and then the viability percentage was calculated as follows

$$\text{viable cells (\%)} = \frac{\text{total number of viable cells per mL}}{\text{total number of cells per mL}} \times 100 \quad (8)$$

Statistically significant differences were determined using one-way analysis of variance (ANOVA) followed by the Bonferroni tests to compare data between groups (Origin Pro 9.0 Software, OriginLab, Northampton, MA). Data are expressed as the mean ± standard deviation (SD). Significant differences were considered at $p < 0.05$.

■ ASSOCIATED CONTENT

Supporting Information

The Supporting Information is available free of charge at https://pubs.acs.org/doi/10.1021/acsomega.0c02212.

Experimental details of the synthesis protocol; characterization procedures; N-type sample characterization; and XPS details of M-type samples (PDF)

■ AUTHOR INFORMATION

Corresponding Author

Jesús Antonio Fuentes-García − *Instituto de Nanociencia de Aragón (INA) & Laboratory of Advanced Microscopies (LMA), Universidad de Zaragoza, 50018 Zaragoza, Spain; Unidad Profesional Interdisciplinaria en Ingeniería y Tecnologías Avanzadas del Instituto Politécnico Nacional, UPIITA-IPN, Ticoman 07340, Mexico;* orcid.org/0000-0003-4952-3702; Email: jesus_spirit69@hotmail.com

Authors

Alex Carvalho Alavarse − *Centro de Ciências Naturais e Humanas, Universidade Federal do ABC, 09210-580 São Paulo, Brazil*

Ana Carolina Moreno Maldonado − *Instituto de Nanociencia de Aragón (INA) & Laboratory of Advanced Microscopies (LMA), Universidad de Zaragoza, 50018 Zaragoza, Spain*

Alfonso Toro-Córdova − *Instituto de Nanociencia de Aragón (INA) & Laboratory of Advanced Microscopies (LMA), Universidad de Zaragoza, 50018 Zaragoza, Spain*

Manuel Ricardo Ibarra − *Instituto de Nanociencia de Aragón (INA) & Laboratory of Advanced Microscopies (LMA) and Departamento de Física de la Materia Condensada, Facultad de Ciencias, Universidad de Zaragoza, 50018 Zaragoza, Spain;* orcid.org/0000-0003-0681-8260

Gerardo Fabián Goya − *Instituto de Nanociencia de Aragón (INA) & Laboratory of Advanced Microscopies (LMA) and Departamento de Física de la Materia Condensada, Facultad de*

Ciencias, Universidad de Zaragoza, 50018 Zaragoza, Spain; orcid.org/0000-0003-1558-9279

Complete contact information is available at: https://pubs.acs.org/10.1021/acsomega.0c02212

Notes

The authors declare no competing financial interest.

■ ACKNOWLEDGMENTS

This work was partially supported by Spanish Ministerio de Ciencia, Innovación y Universidades (Projects RTC-2017-6620-1 and MAT2016-78201-P) and Aragon Regional Government (DGA, Project No. E26). J.A.F.-G. thanks the Mexican Council of Science and Technology (CONACyT) for financial support obtained through postdoctoral fellowship #711124. The authors are indebted to T. E. Torres Molina, E. Lima Jr., and E. Winkler for their technical and scientific support of the EPR analysis. The use of Servicio General de Apoyo a la Investigación (SAI, UNIZAR) is acknowledged. A.T.-C. and A.C.M.-M. acknowledge financial support from the Spanish Ministry of Science through Project RTC-2017-6620-1.

■ REFERENCES

(1) Shafi, K. V. P. M.; Ulman, A.; Yan, X.; Yang, N.-L.; Estournès, C.; White, H.; Rafailovich, M. Sonochemical Synthesis of Functionalized Amorphous Iron Oxide Nanoparticles. *Langmuir* **2001**, *17*, 5093−5097.

(2) Kim, E. H.; Lee, H. S.; Kwak, B. K.; Kim, B. K. Synthesis of Ferrofluid with Magnetic Nanoparticles by Sonochemical Method for MRI Contrast Agent. *J. Magn. Magn. Mater.* **2005**, *289*, 328−330.

(3) Luche, J. L.; Pétrier, C.; Gemal, A. L.; Zikra, N. Ultrasound in Organic Synthesis. 2. Formation and Reaction of Organocopper Reagents. *J. Org. Chem.* **1982**, *47*, 3805−3806.

(4) Blandamer, M. J.; Waddington, D. Ultrasonic Absorption Properties of Binary Aqueous Mixtures. *Adv. Mol. Relax. Processes* **1970**, *2*, 1−40.

(5) Bang, J. H.; Suslick, K. S. Applications of Ultrasound to the Synthesis of Nanostructured Materials. *Adv. Mater.* **2010**, *22*, 1039−1059.

(6) Suslick, K. S. Sonochemistry. *Science* **1990**, *247*, 1439−1445.

(7) Xu, H.; Zeiger, B. W.; Suslick, K. S. Sonochemical Synthesis of Nanomaterials. *Chem. Soc. Rev.* **2013**, *42*, 2555−2567.

(8) Hinman, J. J.; Suslick, K. S. Nanostructured Materials Synthesis Using Ultrasound. *Top. Curr. Chem.* **2017**, *375*, 12.

(9) Nishida, I. Precipitation of Calcium Carbonate by Ultrasonic Irradiation. *Ultrason. Sonochem.* **2004**, *11*, 423−428.

(10) Jordens, J.; Appermont, T.; Gielen, B.; Van Gerven, T.; Braeken, L. Sonofragmentation: Effect of Ultrasound Frequency and Power on Particle Breakage. *Cryst. Growth Des.* **2016**, *16*, 6167−6177.

(11) Kim, H. N.; Suslick, K. S. The Effects of Ultrasound on Crystals: Sonocrystallization and Sonofragmentation. *Crystals* **2018**, *8*, No. 280.

(12) Pokhrel, N.; Vabbina, P. K.; Pala, N. Sonochemistry: Science and Engineering. *Ultrason. Sonochem.* **2016**, *29*, 104−128.

(13) Okoli, C. U.; Kuttiyiel, K. A.; Cole, J.; McCutchen, J.; Tawfik, H.; Adzic, R. R.; Mahajan, D. Solvent Effect in Sonochemical Synthesis of Metal-Alloy Nanoparticles for Use as Electrocatalysts. *Ultrason. Sonochem.* **2018**, *41*, 427−434.

(14) Dang, F.; Kamada, K.; Enomoto, N.; Hojo, J.; Enpuku, K. Sonochemical Synthesis of the Magnetite Nanoparticles in Aqueous Solution. *J. Ceram. Soc. Jpn.* **2007**, *115*, 867−872.

(15) Abu Mukh-Qasem, R.; Gedanken, A. Sonochemical Synthesis of Stable Hydrosol of Fe_3O_4 Nanoparticles. *J. Colloid Interface Sci.* **2005**, *284*, 489−494.

(16) Nazrul Islam, M.; Van Phong, L.; Jeong, J. R.; Kim, C. A Facile Route to Sonochemical Synthesis of Magnetic Iron Oxide (Fe_3O_4) Nanoparticles. *Thin Solid Films* **2011**, *519*, 8277−8279.

(17) Abbas, M.; Takahashi, M.; Kim, C. Facile Sonochemical Synthesis of High-Moment Magnetite (Fe_3O_4) Nanocube. *J. Nanopart. Res.* **2013**, *15*, No. 1354.

(18) Marchegiani, G.; Imperatori, P.; Mari, A.; Pilloni, L.; Chiolerio, A.; Allia, P.; Tiberto, P.; Suber, L. Sonochemical Synthesis of Versatile Hydrophilic Magnetite Nanoparticles. *Ultrason. Sonochem.* **2012**, *19*, 877−882.

(19) Abbas, M.; Abdel-Hamed, M. O.; Chen, J. Efficient One-Pot Sonochemical Synthesis of Thickness-Controlled Silica-Coated Superparamagnetic Iron Oxide (Fe_3O4/SiO_2) Nanospheres. *Appl. Phys. A* **2017**, *123*, No. 775.

(20) Akinwekomi, V.; Maree, J. P.; Zvinowanda, C.; Masindi, V. Synthesis of Magnetite from Iron-Rich Mine Water Using Sodium Carbonate. *J. Environ. Chem. Eng.* **2017**, *5*, 2699−2707.

(21) Snoussi, Y.; Bastide, S.; Abderrabba, M.; Chehimi, M. M. Sonochemical Synthesis of Fe_3O_4@NH_2-Mesoporous Silica@Polypyrrole/Pd: A Core/Double Shell Nanocomposite for Catalytic Applications. *Ultrason. Sonochem.* **2018**, *41*, 551−561.

(22) Balachandramohan, J.; Anandan, S.; Sivasankar, T. A Simple Approach for the Sonochemical Synthesis of Fe_3O_4-Guargum Nanocomposite and Its Catalytic Reduction of p-Nitroaniline. *Ultrason. Sonochem.* **2018**, *40*, 1−10.

(23) Dang, F.; Enomoto, N.; Hojo, J.; Enpuku, K. Sonochemical Synthesis of Monodispersed Magnetite Nanoparticles by Using an Ethanol-Water Mixed Solvent. *Ultrason. Sonochem.* **2009**, *16*, 649−654.

(24) Dolores, R.; Raquel, S.; Adianez, G. L. Sonochemical Synthesis of Iron Oxide Nanoparticles Loaded with Folate and Cisplatin: Effect of Ultrasonic Frequency. *Ultrason. Sonochem.* **2015**, *23*, 391−398.

(25) Iwasaki, T.; Mizutani, N.; Watano, S.; Yanagida, T.; Kawai, T. Size Control of Magnetite Nanoparticles by Organic Solvent-Free Chemical Coprecipitation at Room Temperature. *J. Exp. Nanosci.* **2010**, *5*, 251−262.

(26) Wang, Y.; Nkurikiyimfura, I.; Pan, Z. Sonochemical Synthesis of Magnetic Nanoparticles. *Chem. Eng. Commun.* **2015**, *202*, 616−621.

(27) Chatel, G. How Sonochemistry Contributes to Green Chemistry? *Ultrason. Sonochem.* **2018**, *40*, 117−122.

(28) Suppiah, D. D.; Abd Hamid, S. B. One Step Facile Synthesis of Ferromagnetic Magnetite Nanoparticles. *J. Magn. Magn. Mater.* **2016**, *414*, 204−208.

(29) Pfeiffer, C.; Rehbock, C.; Hühn, D.; Carrillo-Carrion, C.; De Aberasturi, D. J.; Merk, V.; Barcikowski, S.; Parak, W. J. Interaction of Colloidal Nanoparticles with Their Local Environment: The (Ionic) Nanoenvironment around Nanoparticles Is Different from Bulk and Determines the Physico-Chemical Properties of the Nanoparticles. *J. R. Soc. Interface* **2014**, *11*, No. 20130931.

(30) Ravelo-Acuña, D.; Fuentes-García, J. A.; Yee-Madeira, H. T.; Diaz-Cano, A. I.; Goya, G. F.; Santoyo-Salazar, J. Sonochemical Magnetite Encapsulation in Silica at Low Irradiation Power. *Mater. Lett.* **2019**, *250*, 103−107.

(31) Nyquist, R. A. Chapter 5—Sulfoxides, Sulfones, Sulfates, Monothiosulfates, Sulfonyl Halides, Sulfites, Sulfonamides, Sulfonates, and N-Sulfinyl Anilines. *Interpreting Infrared, Raman, and Nuclear Magnetic Resonance Spectra* **2001**, *2*, 85−117.

(32) Iyengar, S. J.; Joy, M.; Ghosh, C. K.; Dey, S.; Kotnala, R. K.; Ghosh, S. Magnetic, X-Ray and Mössbauer Studies on Magnetite/Maghemite Core-Shell Nanostructures Fabricated through an Aqueous Route. *RSC Adv.* **2014**, *4*, 64919−64929.

(33) Li, Y. S.; Church, J. S.; Woodhead, A. L. Infrared and Raman Spectroscopic Studies on Iron Oxide Magnetic Nano-Particles and Their Surface Modifications. *J. Magn. Magn. Mater.* **2012**, *324*, 1543−1550.

(34) Yamashita, T.; Hayes, P. Analysis of XPS Spectra of Fe^{2+} and Fe^{3+} Ions in Oxide Materials. *Appl. Surf. Sci.* **2008**, *254*, 2441−2449.

(35) Lesiak, B.; Rangam, N.; Jiricek, P.; Gordeev, I.; Tóth, J.; Kövér, L.; Mohai, M.; Borowicz, P. Surface Study of Fe_3O_4 Nanoparticles

Functionalized With Biocompatible Adsorbed Molecules. *Front. Chem.* **2019**, *7*, No. 642.
(36) Yang, Y.; Huang, M.; Qian, J.; Gao, D.; Liang, X. Tunable Fe_3O_4 Nanorods for Enhanced Magnetic Hyperthermia Performance. *Sci. Rep.* **2020**, *10*, No. 8331.
(37) Hodych, J. P. Magnetostrictive Control of Coercive Force in Multidomain Magnetite. *Nature* **1982**, *298*, 542−544.
(38) Avolio, M.; Guerrini, A.; Brero, F.; Innocenti, C.; Sangregorio, C.; Cobianchi, M.; Mariani, M.; Orsini, F.; Arosio, P.; Lascialfari, A. In-Gel Study of the Effect of Magnetic Nanoparticles Immobilization on Their Heating Efficiency for Application in Magnetic Fluid Hyperthermia. *J. Magn. Magn. Mater.* **2019**, *471*, 504−512.
(39) Talebi, M.; Balasi, Z. M.; Ahadian, M. M.; Hatamie, S.; Alavijeh, M. H. S.; Ghafuri, H. Biocompatibility and Hyperthermia Efficiency of Sonochemically Synthesized Magnetic Nanoparticles. *SPIN* **2019**, *09*, No. 1940006.
(40) Kaczmarek, K.; Mrówczyński, R.; Hornowski, T.; Bielas, R.; Józefczak, A. The Effect of Tissue-Mimicking Phantom Compressibility on Magnetic Hyperthermia. *Nanomaterials* **2019**, *9*, No. 803.
(41) Calatayud, M. P.; Soler, E.; Torres, T. E.; Campos-Gonzalez, E.; Junquera, C.; Ibarra, M. R.; Goya, G. F. Cell Damage Produced by Magnetic Fluid Hyperthermia on Microglial BV2 Cells OPEN. *Sci. Rep.* **2017**, *7*, No. 8627.
(42) Patil, U. S.; Adireddy, S.; Jaiswal, A.; Mandava, S.; Lee, B. R.; Chrisey, D. B. In Vitro/In Vivo Toxicity Evaluation and Quantification of Iron Oxide Nanoparticles. *Int. J. Mol. Sci.* **2015**, *16*, 24417−24450.
(43) Karlsson, H. L.; Gustafsson, J.; Cronholm, P.; Möller, L. Size-Dependent Toxicity of Metal Oxide Particles-A Comparison between Nano- and Micrometer Size. *Toxicol. Lett.* **2009**, *188*, 112−118.
(44) Manke, A.; Wang, L.; Rojanasakul, Y. Mechanisms of Nanoparticle-Induced Oxidative Stress and Toxicity. *BioMed Res. Int.* **2013**, *2013*, No. 942916.
(45) Patil, R. M.; Thorat, N. D.; Shete, P. B.; Bedge, P. A.; Gavde, S.; Joshi, M. G.; Tofail, S. A. M.; Bohara, R. A. Comprehensive Cytotoxicity Studies of Superparamagnetic Iron Oxide Nanoparticles. *Biochem. Biophys. Rep.* **2018**, *13*, 63−72.
(46) Gas, P.; Miaskowski, A. In *Specifying the Ferrofluid Parameters Important from the Viewpoint of Magnetic Fluid Hyperthermia*, IEEE Conference on Selected Problems of Electrical Engineering and Electronics; 2015.
(47) Calatayud, M. P.; Sanz, B.; Raffa, V.; Riggio, C.; Ibarra, M. R.; Goya, G. F. The Effect of Surface Charge of Functionalized Fe_3O_4 Nanoparticles on Protein Adsorption and Cell Uptake. *Biomaterials* **2014**, *35*, 6389−6399.

https://dx.doi.org/10.1021/acsomega.0c02212
ACS Omega 2020, 5, 26357−26364